The importance of specifically adsorbed ions for electrokinetic phenomena
Bridging the gap between experiments and MD simulations

Döpke, Max F.; Hartkamp, Remco

Important note
To cite this publication, please use the final published version (if applicable).
Please check the document version above.

The importance of specifically adsorbed ions for electrokinetic phenomena: Bridging the gap between experiments and MD simulations ⒡

Max F. Döpke, and ⓘD Remco Hartkamp

COLLECTIONS

Paper published as part of the special topic on Fluids in Nanopores

⒡ This paper was selected as Featured

ARTICLES YOU MAY BE INTERESTED IN

The importance of specifically adsorbed ions for electrokinetic phenomena: Bridging the gap between experiments and MD simulations ⓕ

Max F. Döpke and Remco Hartkamp[a] ⓘD

AFFILIATIONS

Process & Energy Department, Delft University of Technology, Leeghwaterstraat 39, 2628 CB Delft, The Netherlands

Note: This paper is part of the JCP Special Topic on Fluids in Nanopores.
[a]Author to whom correspondence should be addressed: r.m.hartkamp@tudelft.nl

ABSTRACT

Molecular Dynamics (MD) simulations are uniquely suitable for providing molecular-level insights into the Electric Double Layer (EDL) that forms when a charged surface is in contact with an aqueous solution. However, simulations are only as accurate in predicting EDL properties as permitted by the atomic interaction models. Experimental ζ-potential values and surface charges could provide a potentially suitable reference to validate and tune the interaction models, if not for the fact that they themselves are a product of imperfect models used to interpret the raw measurement data. Here, we present an approach to tune an interaction model by comparing Electro-Osmotic Flow (EOF) MD simulations against experimental Streaming Current (SC) measurements while minimizing potential modeling errors arising from both approaches. The point that is least susceptible to interpretation and modeling errors is argued to be at the concentration for which zero flow velocity is observed in EOF simulations and a net zero electric current is measured in SC experiments. At this concentration, the ζ-potential is also zero. We were able to match the experimental concentration at which $\zeta = 0$ in MD simulations for a $CaCl_2$ solution at pH 7.5 in contact with fused silica by tuning the ion-surface Lennard-Jones cross interactions. These interactions were found to greatly affect the ion distribution within the EDL and particularly the formation of inner-sphere surface-complexes, which, in turn, affects the electrokinetic flow. With the ion distribution determined explicitly, a series of properties can be calculated unambiguously, such as the capacitance needed for surface complexation models.

I. INTRODUCTION

An oxide in contact with an aqueous solution adopts a bare surface charge density that is balanced by ions forming a Stern layer and a diffuse layer near the solid–liquid interface. This so-called Electric Double Layer (EDL) plays an important role in geology,[1] materials science,[2] biology,[3] and electrochemistry.[4] It controls, for example, the capacitance in batteries, colloidal stability,[5] and dissolution of materials and can be used for ion sensing.[6] A detailed understanding of the EDL and its dependence on the solid material, solution composition, and pH is thus invaluable. However, no single experimental technique can measure its entire structure and dynamics. Instead, partial pieces of the puzzle can be gleaned from a variety of different techniques. Potentiometric titration[7] can be used to measure the bare surface charge density, while the effective surface charge density can be inferred through force measurements[8] or electrokinetics.[9] Electrokinetic techniques can also provide information about the mobility of ions within the EDL, and spectroscopic techniques[10–12] can be used to infer information about the interfacial ion and water distribution and orientation. Ideally, a comprehensive picture of the EDL for a given solid–liquid interface could be constructed by combining multiple techniques in a single device to exclude the possibility of differences in material sample or experimental conditions. Although some techniques

have indeed been integrated together,[13,14] this is a very difficult task and not all techniques can be carried out under the same conditions and setups. For instance, force measurements require access to the substrate, while some electrokinetic techniques require closed channels.

Another fundamental challenge of acquiring a detailed understanding of the EDL from a combination of experimental techniques is their dependence on models to interpret measurements.[15,16] Consequently, an inferred charge or potential or other EDL property is inherently biased by the assumptions and parameters used in the model, with the accuracy of models depending also on the experimental conditions. For example, the Helmholtz–Smoluchowski theory is known to become inaccurate for small colloidal particles and at low ion concentrations, where the effects of surface conductance compared to the bulk conductance are large.[17,18] On the other hand, the widely used Gouy–Chapman model is known to break down under conditions of strong electrostatic coupling. The consequences of modeling inaccuracies show, for example, discrepancies between ζ-potentials obtained via multiple approaches.[19–21]

The standard approaches that are used to interpret experiments are especially put to the test when dealing with high ion concentrations and multivalent electrolytes. An interesting phenomenon that can occur under such conditions is the reversal of the sign of the diffuse layer charge. This reversal is known as charge inversion. Experimentally, the diffuse layer charge can be inferred through, for example, electrokinetic techniques,[9] force measurements,[8] or non-linear optics,[22,23] but the results between these methods differ from each other. In electrokinetics, for instance, an assumption on the ion density profiles in the diffuse layer is required, while in force measurements the tip itself may influence this very profile, and in non-linear optics the interpretation and relation between the measured quantities and EDL structure remains challenging. Even between different electrokinetic techniques, such as Streaming Currents (SC), streaming potentials, electro-acoustics, or Electro-Osmotic Flow (EOF), results may differ.[19–21] To better understand charge inversion, and more generally the EDL structure and dynamics under these conditions, a high-resolution model-free approach is needed.

Having access to all atomic positions, velocities, forces, and energies, Molecular Dynamics (MD) simulations have the unique potential to provide a high-resolution and model-free comprehensive three-dimensional picture of the EDL structure and dynamics.[24] However, this requires confidence that the description of atomic interactions, which is the key required input to the simulations, does in fact produce the correct behavior. MD studies of solid–liquid interfaces have shown a diverse picture, with ion adsorption varying largely between studies.[25–36] For example, Lorenz et al.[26] predicted charge inversion in silica nanochannels with a bare surface charge density of -144 mC/m^2 filled with 200 mmol/l CaCl$_2$, while Biriukov et al.[36] predicted no charge inversion under similar conditions. In fact, many MD simulation studies predict charge inversion at bulk ion concentrations much lower than inferred from experiments.[25,26,35] One important cause of the deviations between ion adsorption in different MD simulation studies and their deviation from experiments is the fact that the Lennard-Jones cross interactions required to describe solid–liquid interactions are typically not part of the force field optimization. With a few exceptions,[37]

these are rather estimated based on common combination rules. Rigorous optimization of these parameters would require unambiguous and detailed target data on the interfacial distribution and adsorption of ions onto the surface, which is not directly measurable. Another cause of the deviations is the use of full charges. These do not take into account the dielectric screening of the medium and frequently result in an over-prediction of ion-adsorption[37,38] and ion-pairing.[39,40] In an attempt to account for this screening, the Electronic Continuum Correction (ECC) theory states that the charges should be scaled by a factor between 0.75 and 0.85.[39] While strictly speaking this charge scaling only applies to homogeneous systems with a constant dielectric,[41] its use in interfacial systems with a variable dielectric has shown very promising improvements in the description of solid–liquid interactions.[36,38]

In this study, we propose a scaling of the Lennard-Jones cross interactions as a free variable combined with the use of ECC to achieve good agreement between nonequilibrium MD simulations and electrokinetic experiments. Specifically, we tune the solid-ion Lennard-Jones cross interactions to match the concentration at which $\zeta = 0$ for both electrokinetic experiments and electrokinetic simulations. At this concentration, the measured properties (i.e., electrical current or flow velocity) tend to zero, resulting in $\zeta = 0$ via the Helmholtz–Smoluchowski theory regardless of fluid properties such as viscosity, thereby providing a concentration that is least susceptible to interpretation. We examine the proposed approach in a fused silica slit pore filled with a CaCl$_2$ electrolyte at pH 7.5. The reason we choose this system is twofold: first, experimental SC data are available,[9] including a concentration at which $\zeta = 0$, and second, it is a relevant system for natural processes and industrial applications.[42] We find that the number of specifically adsorbed ions is the key property to determine the experimental concentration at which $\zeta = 0$. Once the simulations are tuned and validated, we provide detailed insights into the EDL structure and dynamics, which can be used for future improvements of surface complexation and continuum models.

The remainder of the paper is organized as follows: The theoretical framework and MD simulation set-up are presented in Sec. II. The results are discussed in Sec. III. Finally, the conclusions are provided in Sec. IV.

II. METHODS

A. Theoretical framework

Here, we lay out the most common theoretical framework to calculate the ζ-potential through either SC or EOF experiments shown in Fig. 1 and described in more detail in Delgado et al.[17]

1. Streaming current experiments

A typical SC experiment is displayed in the bottom part of Fig. 1. A pressure gradient $\Delta p_x/L$ is applied, resulting in a planar Poiseuille flow profile $u_x(z)$ (parabolic flow profile). A charge density imbalance $\rho_e(z)$ in the diffuse layer of the EDL causes a measurable electric current I_{str}. If the bare surface is negatively charged, an excess of cations is expected in the mobile part of the EDL, resulting in a positive I_{str}. In the event of charge inversion, however, the immobile part of the EDL overcompensates the bare surface charge
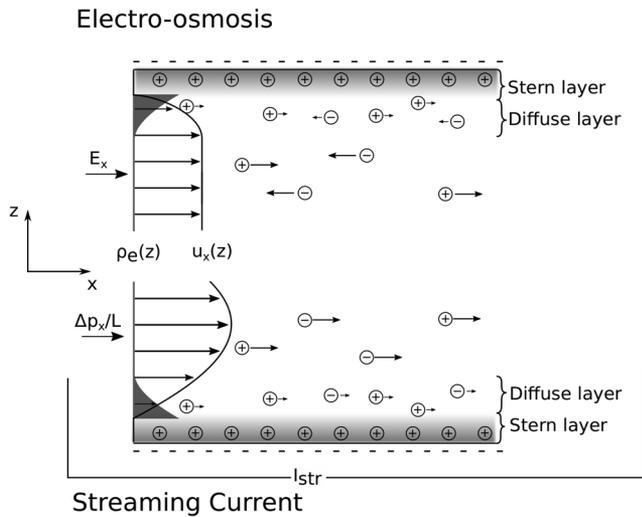
FIG. 1. Schematic of an Electro-Osmotic Flow (EOF) experiment (top) and a Streaming Current (SC) experiment (bottom).

density, resulting in an excess of mobile anions in the EDL, reversing the sign of I_{str}.

In order to determine the ζ-potential, let us relate I_{str} to $\rho_e(z)$ and $u_x(z)$ in a duct of width w, height $2h$ ($-h$ to h), and length L via

$$I_{str} = 2w \int_0^h \rho_e(z) u_x(z) dz, \qquad (1)$$

with $\rho_e(z)$ being described by the Poisson equation,

$$\varepsilon_0 \varepsilon_r \frac{d^2 \psi(z)}{dz^2} = -\rho_e(z), \qquad (2)$$

assuming a constant dielectric permittivity ε_r, and $u_x(z)$ being given by the planar Poiseuille flow solution,

$$u_x(z) = \frac{\Delta p_x}{2\eta L}\left(h^2 - z^2\right), \qquad (3)$$

assuming a constant viscosity η. ε_0 and ψ are the vacuum permittivity and electrostatic potential, respectively. Substituting Eqs. (2) and (3) into (1), twice integrating by parts, applying boundary conditions $\psi(z_{no\text{-}slip}) = \zeta$ and $\psi(z_{bulk}) = 0$, and rearranging for ζ [see Eq. (S1) in the supplementary material] yields[43]

$$\zeta = -\frac{\eta}{\varepsilon_0 \varepsilon_r 2wh} \frac{L}{\Delta p_x} I_{str}. \qquad (4)$$

2. Electro-osmotic flow experiments

The top part of Fig. 1 displays a typical EOF experiment. An external electric field E_x is applied parallel to the walls, accelerating

cations in the direction of the electric field and anions in the opposite direction. Water molecules are dragged along due to viscous forces. The competing effects of cations and anions on the overall flow is balanced in the electroneutral [$\rho_e(z) = 0$] bulk region of the channel. This neutrality does not apply near the surface, where an excess of mobile cations or mobile anions accelerates the fluid along or against the electric field, respectively. This results in a plug flow $u_x(z)$, as shown in the top of Fig. 1, governed by the 1D Navier–Stokes momentum equation,

$$\eta \frac{d^2 u_x(z)}{dz^2} = -\rho_e(z) E_x, \qquad (5)$$

with boundary conditions $u_x(z_{no\text{-}slip}) = 0$ and $u_x(z_{bulk}) = u_{x,bulk}$. Combining this relation with the 1D Poisson equation given in Eq. (2), with the boundary conditions $\psi(z_{no\text{-}slip}) = \zeta$ and $\psi(z_{bulk}) = 0$, an expression for the velocity profile is obtained,

$$u_x(z) = \frac{\varepsilon_0 \varepsilon_r E_x}{\eta}\left(\psi(z) - \zeta\right). \qquad (6)$$

For the velocity in the bulk, this equation reduces to the Helmholtz–Smoluchowski equation,

$$\zeta = -\frac{\eta u_{x,bulk}}{\varepsilon_0 \varepsilon_r E_x}, \qquad (7)$$

relating the measurable bulk velocity $u_{x,bulk}$ to the ζ-potential.

3. Similarity between SC and EOF experiments

Considering that SC and EOF experiments are both performed within the linear response regime, the no-slip plane (separation between the Stern layer and the diffuse layer in Fig. 1) and adsorption of ions are independent of flow. Consequently, $\rho_e(z)$, $\psi(z)$, and the ζ-potential should also be identical in both SC and EOF experiments. Despite this, results have deviated between electrokinetic techniques.[19–21] One exception is the combinations of concentration and pH at which $\zeta = 0$, which are rather uniformly predicted. When observing Eqs. (4) and (7), this is also not surprising, since when $I_{str} \to 0$ or $u_{x,bulk} \to 0$ the dependence of $\zeta \to 0$ on properties such as the viscosity, dielectric, or duct size and shape vanishes. Therefore, the fact that differences arise between finite ζ-potential values predicted from these methods is thought to be, for example, due to the use of a planar Poiseuille flow solution [Eq. (3)]. Other possible sources of error are the assumption of constant dielectric permittivity or viscosity, measurement noise, the use of differing theoretical models, differences in the treatments of the individual substrates, and contaminants. Furthermore, some authors have also suggested that the surface properties may be affected by the flow.[44,45]

B. Molecular Dynamics simulations

We perform non-equilibrium MD simulations of $CaCl_2$ electrolytes in an amorphous silica slit pore. The pore is generated following our previous work.[35] In short, we prepare a block of amorphous silica by annealing and quenching a β-cristobalite using

the BKS force field.[46] For all other simulations, the Interface Force Field[47] (IFF) is used for silica. The block is cut in the middle, creating 2 opposing surfaces with dangling oxygens. The dangling oxygens are protonated and the silanol (SiOH) density is adjusted to ~5 SiOH/nm² by bridging some of the nearby SiOH groups. Finally, TIP4P/2005 water molecules[48] and Madrid-2019 ions[40] are added between the slabs, and the surface charge density is adjusted by deprotonating a given number of silanol sites corresponding to a pH of ~7.5.

As seen from potentiometric titration data[49,50] in Fig. 2, maintaining a constant surface charge density across a bulk ion concentration range or when comparing different ionic compounds does not represent the experimentally relevant scenario in which pH is kept constant. Yet, such a constant surface charge is standard practice in MD simulation studies. Alternatively, in order to indirectly account for a constant pH, we vary the bare surface charge density σ_0 together with the bulk ion concentration c_0. Since the surface charge density of amorphous silica is governed by discretely deprotonated SiOH (SiO⁻) groups, not every bare surface charge density is possible in our system with either wall having a surface area of ~12 nm². The black dashed line in Fig. 2 displays the possible bare surface charge densities in our system by deprotonating a discrete number of SiOH on each surface. The green crosses mark the simulation conditions that are studied here. Within the simulation, the net charge of each SiO⁻ group is scaled down by a factor of 0.85 in order to be consistent with the charge scaling of the Madrid-2019 force field. We remark that this is a purely computational consideration and full charges are used during post-processing with the exception of streaming velocities that are scaled up by a factor of 1/0.85. This scaling of the streaming velocity is necessary since the scaling down of ionic charges by 0.85 is equivalent to an ion with the nominal charge experiencing a reduced electric field $E_{x,\text{eff}} = 0.85 E_x$.[36]

The density of the fluid is adjusted by pushing the walls toward each other with a force equivalent to 1 bar nominal pressure for 20 ns. The resulting bulk densities and concentrations calculated from
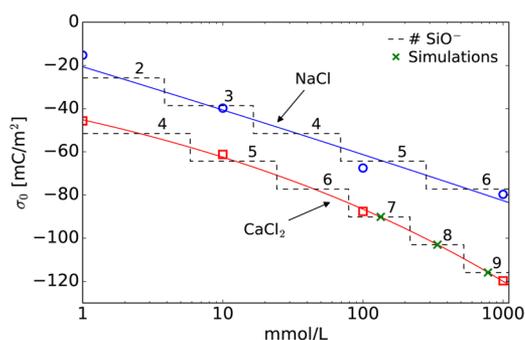
FIG. 2. Experimental results of bare surface charge density σ_0 against bulk ion concentration c_0 from surface charge titration experiments on ground quartz[49] (1 mM, 10 mM, and 100 mM) and amorphous silica[50] (1000 mM) at constant pH of 7.5. NaCl is provided as a reference. The full lines are a power law fit of the experimental data points, and the dashed lines represent the number of SiO⁻ per surface that would correspond to the respective bare surface charge density with our system.

a subsection in the center of the channel are shown in Fig. S1 in the supplementary material. Subsequently, the position of the walls is fixed in space, and an electric field of $E_x = 0.2$ V/nm is applied to the fluid. Such a large electric field is necessary in MD simulations to increase the signal to noise ratio (Fig. S2 shows that the resulting flow is still within the linear response regime).[31,34,51,52] Note that simulating EOF is preferred over SC for our purpose since the relation between the streaming current and the ζ-potential depends on the channel height [Eq. (4)], which is not uniquely defined for atomistic surfaces with a finite roughness. This ambiguity affects MD simulations of SC much more than experiments because of the typically much smaller channel heights in MD simulations. On the other hand, EOF simulations are unaffected by this ambiguity.

The temperature in the system is maintained by connecting the walls to a thermal heat bath at 298 K via a Nosé–Hoover thermostat. This is shown to yield a fluid temperature of 295 K in Fig. S3. Simulations with an externally applied electric field are equilibrated for 20 ns followed by production runs of 100 ns at a time step of 2 fs. Two independent simulations with different amorphous surfaces and starting conditions are performed for all configurations. All simulations are performed with Large-scale Atomic/Molecular Massively Parallel Simulator (LAMMPS)[53] using a cut-off of 12 Å and the particle–particle particle–mesh long-range electrostatic solver[54] with a precision of 1×10^{-4}. OH bonds of water and silanols and HOH angles of water are constrained using the SHAKE algorithm[55] with a precision of 1×10^{-4}. Periodic boundary conditions are used in x and y. In the z direction, a vacuum equal to 3 times the box length is introduced beyond the walls to remove dipole inter-slab interactions using the algorithm from Yeh and Berkowitz.[56] The final systems are described in Table I. The channel heights $2h$ are chosen in order to avoid EDL overlap.

Cross interactions within each force field (IFF and Madrid-2019 including TIP4P/2005) are applied as recommended by the respective authors. Between the force fields, however, this leaves the open question of what combination rule to use. Between TIP4P/2005 and IFF, we use the Lorentz Berthelot[57] (LB) combination rule. However, since the Madrid-2019 Ca²⁺–O_water and Cl⁻–O_water Lennard-Jones cross interactions are specifically defined, we investigate various Lennard-Jones cross interactions between the Madrid-2019 ions and IFF oxygen atoms following the scaling,

$$A_{X-O_{IFF}} = A_{X-O_{IFF}}^{LB}\left[\left(\frac{A_{X-O_{water}}}{A_{X-O_{water}}^{LB}} - 1\right)f + 1\right], \quad (8)$$

with $A \in \{\sigma, \varepsilon\}$ and $X \in \{\text{Ca}^{2+}, \text{Cl}^-\}$. The scaling is applied simultaneously to σ and ε and to both Ca²⁺ and Cl⁻ ions.

TABLE I. Channel system configurations. c_0 is the bulk CaCl₂ concentration, A_s is the surface area, $2h$ is the channel height (approximate separation between the surfaces), and # denotes the number of SiO⁻ per surface, H₂O molecules, Ca²⁺ ions, and Cl⁻ ions.

c_0 (mmol/l)	A_s (nm²)	$2h$ (nm)	# SiO⁻	# H₂O	# Ca²⁺	# Cl⁻
150	12	14	7	5733	22	30
380	12	6	8	2457	24	32
800	12	6	9	2457	44	70

III. RESULTS

In this section, we show first the impact of scaling the solid–liquid interactions on the ion distribution within the EDL, followed by a comparison with experiments and discussion relating the EDL structure to the observed EOF. Finally, the mobility within the EDL is assessed.

A. Scaling solid–liquid interactions

The bare surface charge density of amorphous silica at a given pH and concentration is screened by ions. We distinguish for each ion between 4 different adsorption types, namely, Inner-Sphere Surface-Complexes (ISSC), Outer-Sphere Surface-Complexes (OSSC), ions within the diffuse layer, and free ions, as shown in Fig. 3(a). ISSC and OSSC are ions for which a surface atom (Si, O, and H) is part of their first or second hydration shell, respectively. Ions within the diffuse layer are defined as having their first 2 hydration shells intact, but remaining within 12 Å of the surface (defined as the distance between nuclei of ions and nuclei of the nearest surface atom).[35] Note that the 12 Å length is chosen rather arbitrarily to represent the real diffuse layer approximately. Free ions are those which are farther than 12 Å from the surface. Varying the scaling parameter f in Eq. (8), we can control the number of Ca^{2+} ions forming ISSC. Figure 3(b) shows an increase in ISSC formation with a change from $f = 0$ to $f = 1$. As a direct consequence, the formation of OSSC and the number of Ca^{2+} ions in the diffuse layer are reduced. On the other hand, in Fig. 3(c) for Cl^-, the number of ions forming ISSC and OSSC and number of ions within the diffuse layer are found to increase with increasing f. We attribute this to the increased ion–ion correlations resulting from the increase of Ca^{2+} ions forming ISSC, rather than being a direct consequence of the scaled Cl^-–surface interactions. Although direct Cl^- adsorption in the form of ISSC may be unexpected, their existence has been suggested from x-ray experiments.[58]

In Fig. 4, we quantify the effect of f on ISSC and OSSC formation. We run additional simulations at $f = 0.75$ (800 mmol/l only) and $f = 0.9$ and fit the relative charge contribution of ions forming ISSC and OSSC with a power function $\sigma/\sigma_0 \approx af^b + c$. Between $f = 0$ and $f \approx 0.5$, no change in ISSC and OSSC formation is appreciable. Between $f \approx 0.5$ and $f \approx 0.8$, the ISSC contribution increases slightly for all concentrations considered, from 0% up to 16%. The OSSC contribution in return is reduced by 5%–7%. From $f \approx 0.8$ to $f = 1$, a steep increase in σ_{ISSC}/σ_0 and a steep decrease in σ_{OSSC}/σ_0 are observed. At 800 mmol/l, the ISSC contribution even overscreens the surface charge, meaning $\sigma_{ISSC}/\sigma_0 > 1$. Here, σ_0 denotes the bare surface charge density, and σ_{ISSC} and σ_{OSSC} denote the charge density contribution from ions forming ISSC and OSSC, respectively.

B. Comparison with experiments and previous MD results

1. ζ-potential

We have thus far established that varying f affects the number of ions forming ISSC and OSSC. Next, we will determine what value
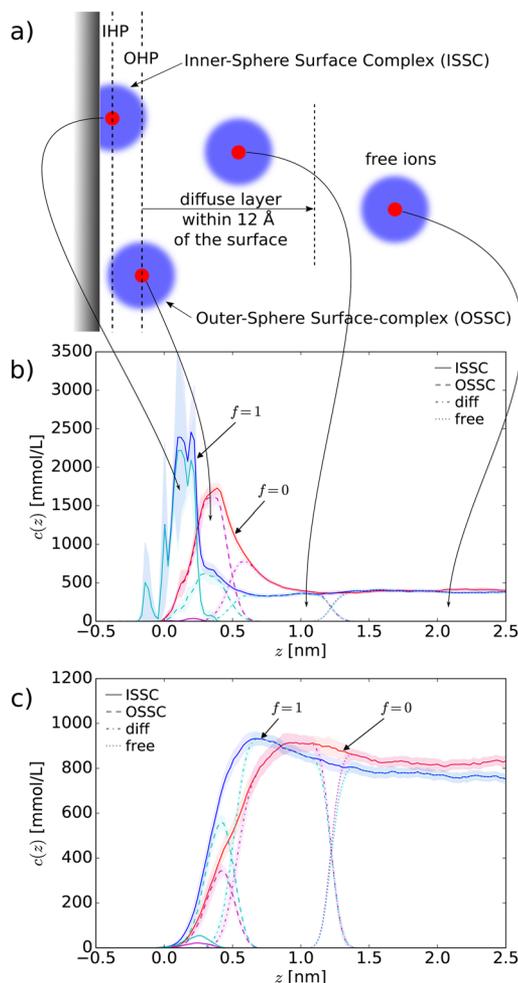
FIG. 3. (a) Classification of adsorption type of ions into Inner-Sphere Surface-Complexes (ISSC), Outer-Sphere Surface-Complexes (ISSC), those within the diffuse layer, and free ions that form part of the bulk. IHP and OHP are the Inner- and Outer-Helmholtz Planes, which are commonly defined as passing through the nuclei of ions forming ISSC and OSSC, respectively. (b) Ca^{2+} and (c) Cl^- concentration profiles $c(z)$ normal to the surface at a bulk $CaCl_2$ concentration c_0 of ~380 mmol/l. $z = 0$ corresponds to the average hydrogen location at the surface. The confidence intervals are 68%.

of f yields good agreement with experimental data for the silica-electrolyte systems studied here. From previous MD studies,[34,59] we know that ions forming ISSC may be considered as virtually immobile. The scaling factor f, therefore, controls via the adsorption also the mobility within the EDL. We postulate that an f exists at which the right amount of immobile adsorbed ions is found to reproduce the experimental ζ-potential measurements.

In Fig. 5(a), we compare the ζ-potential at various concentrations between our EOF simulations, the SC experiments of van der
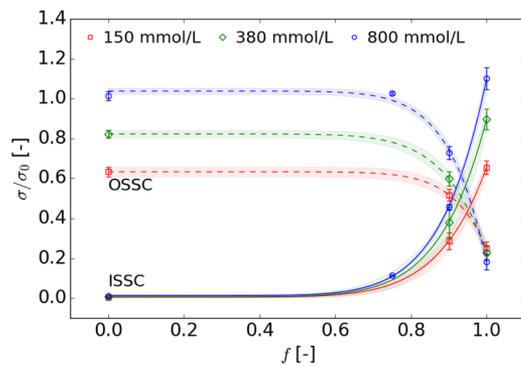
FIG. 4. Relative charge contribution of ions (Ca^{2+} and Cl^-) forming ISSC and OSSC (σ_{ISSC}/σ_0 and σ_{OSSC}/σ_0) as a function of the scaling parameter f for bulk $CaCl_2$ concentrations of 150 mmol/l, 380 mmol/l, and 800 mmol/l. The confidence intervals are 68%.

Heyden *et al.*,[9] and Rashwan *et al.*,[60] the Atomic Force Microscopy (AFM) experiments from Siretanu *et al.*,[8] and previous MD results from EOF and SC simulations from Lorenz *et al.*[26] and EOF simulations from Biriukov *et al.*[36] Compared to the results from
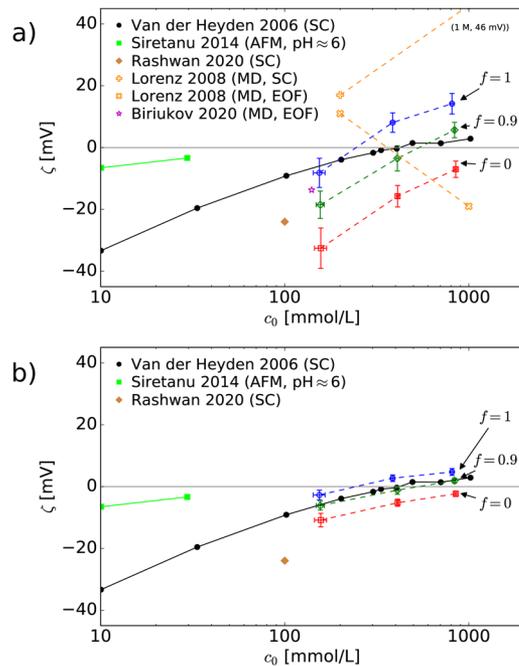
FIG. 5. ζ-potential as a function of $CaCl_2$ bulk concentration c_0 at pH 7.5. Full lines and full symbols denote experiments, and dashed lines and open symbols denote simulations. (a) The TIP4P/2005 water model viscosity and dielectric are used in the Helmholtz–Smoluchowski equation [Eq. (7)] for our simulation results [$f = (0, 0.9, 1)$]. (b) The ζ-potential of (a) from our simulations is divided by 3. The confidence intervals are 68%.

Lorenz *et al.*,[26] our results for the different f-values and the simulation data from Biriukov *et al.*[36] are in reasonable agreement with the experimental results from van der Heyden *et al.*[9] and Rashwan *et al.*[60] Notably, there is a considerable difference between ζ-potentials found by van der Heyden *et al.*[9] and Rashwan *et al.*[60] at 100 mmol/l. Comparable differences are found between values obtained from different electrokinetic techniques. For example, Szymczyk *et al.*[19] found that ζ-potentials from EOF and streaming potential experiments for a NaCl solution in a ceramic channel are increasingly dissimilar at an increasing ion concentration and constant pH, up to $\zeta_{EOF}/\zeta_{SP} \approx 2$ at 10 mmol/l of NaCl. On the other hand, the concentration and pH combination at which $\zeta = 0$ were shown to vary little between EOF and streaming potential experiments, for both NaCl and $CaCl_2$ solutions. These findings have two important implications. First, the concentration of $\zeta = 0$ can be obtained without relying on extensive knowledge or assumptions about the nanoconfined fluid properties and the relation between ζ-potential and fluid transport. This makes this concentration uniquely suitable to tune the MD cross interaction scaling factor f, as we will do in the following. Second, the consistent isoelectric point between the EOF and streaming potential experiments rules out significant differences in surface sample or environmental conditions, suggesting that the differences between the finite ζ-potential values mainly originate from inaccuracies in the linear relationship between the ζ-potential and the measured quantities [i.e., Eqs. (4) and (7)] and in the fluid coefficients used in these models. As such, finite ζ-potential values, and thus the slope of the curves in Fig. 5(a), are less suitable as a means to validate MD results against experimental data. In an analogy to the isoelectric point, which is the pH at which $\zeta = 0$ for a fixed concentration, we will call the concentration at which $\zeta = 0$ for a fixed pH the Isoelectric Concentration (IEC).

We were able to reproduce the IEC (≈ 400 mmol/l for a $CaCl_2$ electrolyte in a fused silica slit pore at pH 7.5)[9] in our simulations almost perfectly by setting $f = 0.9$. With $f = 0$ (thus the standard LB mixing rule) the IEC is overpredicted, while with $f = 1$ it is underpredicted. Furthermore, in Fig. 5(b), we show that by scaling the ζ-potential to a third of its value, also good agreement in the slope between the SC experiments of van der Heyden *et al.*[9] and our EOF simulations can be achieved. This is equivalent to reducing the viscosity in confinement to a third of its bulk value. Such a reduction is unexpected but has been reported in MD simulations depending on the method of determining the viscosity.[61] However, this is difficult to believe as the flow velocity can be shown to be independent of channel width,[51] and an enhancement of viscosity near the surfaces is generally expected and predicted (i.e., viscoelectric and electroviscous effects).[31,62–65] In a similar fashion, a local increase of the dielectric permittivity can also explain the disagreement. A misrepresentation of the concentration-dependent ion diffusion coefficients may be yet another factor affecting the slope. For example, the Madrid-2019 Ca^{2+} diffusion at infinite dilution has been found to be overpredicted by 12%, while at 500 mmol/l it was underpredicted by 20%. From similar simulations, the Cl^- diffusion was found to be underpredicted by 21% at infinite dilution and 40% at 500 mmol/l.[40,66–69] This may corrupt the transfer of velocity from ions to water molecules through viscous forces. As a result, we argue the difference in slope to be due to modeling errors, either of the force field itself, differences between

the experimental and simulation conditions, or differences arising from the models used in EOF and SC experiments and simulations [Eqs. (7) and (4)].

In conclusion, only the isoelectric point and concentration can be used to compare results between various electrokinetic techniques and between simulations and experiments unambiguously. Here, $f = 0.9$ is shown to yield the correct IEC in our simulations and will, therefore, be used in the remainder of this paper. We do, however, not exclude that f may, in fact, be concentration or pH dependent.

2. From ζ-potential to effective surface charge

Similar to the ζ-potential, which is defined as the electrochemical potential at the no-slip plane [$\zeta = \psi(z_{\text{no-slip}})$], the effective surface charge density σ^* is defined as the charge density at the no-slip plane $\Gamma(z_{\text{no-slip}})$. The effective surface charge density is calculated in various experimental studies using electrokinetic techniques or force measurements, making it a potentially suitable means for comparison. From an experimental point of view, the effective surface charge density σ^* and the ζ-potential can be directly related via the Grahame equation,[70,71]

$$\sigma^* = \sqrt{8c_0\varepsilon_0\varepsilon_r k_B T} \sinh\left(\frac{ve\zeta}{2k_B T}\right), \qquad (9)$$

with k_B being the Boltzmann constant, T the temperature, e the elementary charge, and v the ion valency (2 for Ca^{2+} and 1 for Cl^-). This relation suggests that the events of charge inversion and ζ-potential inversion are directly related. However, this hinges on several assumptions. First of all, the charge density distribution is assumed to follow a Boltzmann distribution,[72] neglecting ion–ion correlations and considering ions as point charges. Consequently, it is only valid at small concentrations and can also not reproduce phenomena such as crowding and charge inversion. Furthermore, the derivation of the Grahame equation only applies to symmetric electrolytes. Despite these limitations, the Grahame equation is also frequently used at high concentrations and for asymmetric electrolytes. We note that the effect of using asymmetric electrolytes and treating these as symmetric in the Grahame equation is in fact very small as shown in Fig. S4 by comparing the Grahame equation against a variation for asymmetric electrolytes.[73]

A more precise way of determining σ^* is by extracting it directly from the screening function[31,35,59] $\sigma^* = \Gamma(z_{\text{no-slip}})$ given by Eq. (10),

$$\Gamma(z) = \sigma_0 + \int_0^z \rho_e(z')dz'. \qquad (10)$$

However, this is only possible when $\rho_e(z)$ and $z_{\text{no-slip}}$ are known. In MD simulations, $\rho_e(z)$ can be determined [Fig. 6(a)], but no rigorous method exists to determine the no-slip plane ($z_{\text{no-slip}}$). One could, for example, try to determine this plane from ion mobilities or flow profiles [Fig. 6(d)]. However, the flow profiles near amorphous silica have undulations and even regions of local flow reversal. In some cases, also multiple no-slip planes could be defined.
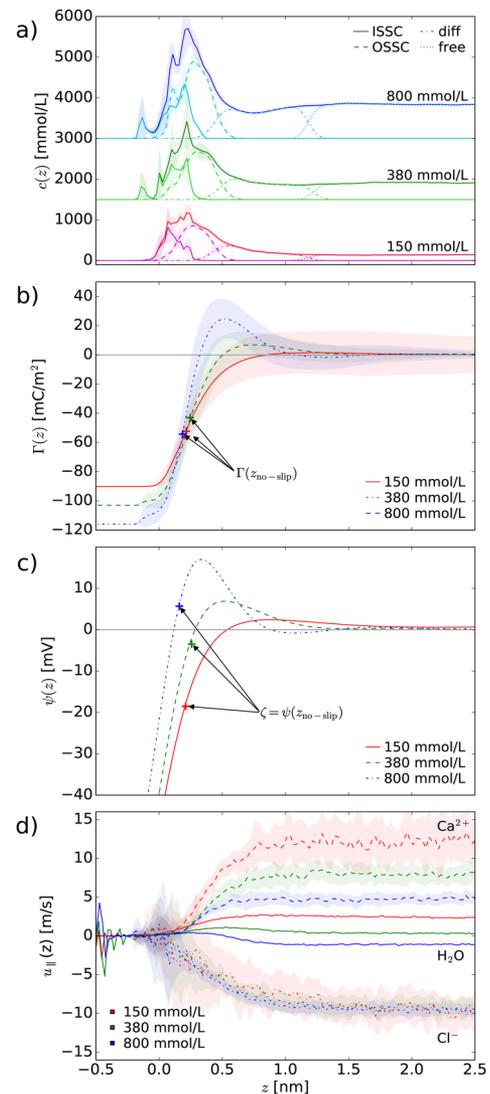
FIG. 6. MD simulation results for $f = 0.9$ at 150 mmol/l, 380 mmol/l, and 800 mmol/l as a function of coordinate z normal to the surface. $z = 0$ corresponds to the average hydrogen location at the surface. (a) Ca^{2+} concentration profile dividing ions into ISSC, OSSC, those within the diffuse layer, and free ions. (b) Screening function from Eq. (10). (c) Electrochemical potential obtained from the Poisson equation [Eq. (2)] and ζ-potential obtained from EOF simulations using the Helmholtz–Smoluchowski equation [Eq. (7)]. (d) Scaled velocity profiles (multiplied by 1/0.85) of Ca^{2+}, Cl^-, and H_2O when an electric field of $E_x = 0.2$ V/nm is applied. The confidence intervals are 68%.

Perhaps, the most rigorous method to determine $z_{\text{no-slip}}$ is to compute the intersection between the electrostatic potential $\psi(z)$ and the ζ-potential [Fig. 6(c)]. Where the ζ-potential is obtained from the Helmholtz–Smoluchowski equation and $\psi(z)$ from the Poisson equation with boundary conditions $d\psi(z_{\text{wall}})/dz = -\sigma_0/\varepsilon_0\varepsilon_r$

and $\psi(z_{\text{bulk}}) = 0$. Note that in the calculation of $\psi(z)$, full charges are used, while the ζ-potential is determined considering a streaming velocity that is scaled up by $1/0.85$. The resulting $z_{\text{no-slip}}$ are added as + symbols in Figs. 6(b) and 6(c). While $z_{\text{no-slip}} \approx 0.2$ nm is nearly the same for all 3 concentrations, it is not really a plane of zero velocity [Fig. 6(d)]. Furthermore, the resulting $\Gamma(z_{\text{no-slip}})$ is considerably lower than $\sigma^*_{\text{Grahame}}$ as shown in Fig. 7(a).

Alternatively, we could use the common assumption that the no-slip plane is within 1 Å of the Outer-Helmholtz Plane[74] (OHP), which is defined as passing through the nuclei of ions forming OSSC [see Fig. 3(a)]. On an amorphous surface, this opens up room for interpretation of the meaning and location of the OHP. From Fig. 6(b), the location of the OHP could be understood as coinciding with the maximum in the OSSC density, the intersection between the OSSC and diffuse layer densities, or the end of the OSSC region, resulting in $z_{\text{no-slip}} \approx 0.3$, $z_{\text{no-slip}} \approx 0.5$, and $z_{\text{no-slip}} \approx 0.6$ nm, respectively, contributing to a very ambiguous definition of $z_{\text{no-slip}}$. In fact, the existence of a single no-slip plane is under most circumstances, as for our system, illusory.

Instead of dwelling on a physical location for the OHP, we calculate the charge contribution associated with the OHP directly from the number of ions forming ISSC and OSSC. Figure 7(a) shows that this definition also yields reasonable agreement with the Grahame equation Eq. (9) and the experimental data.
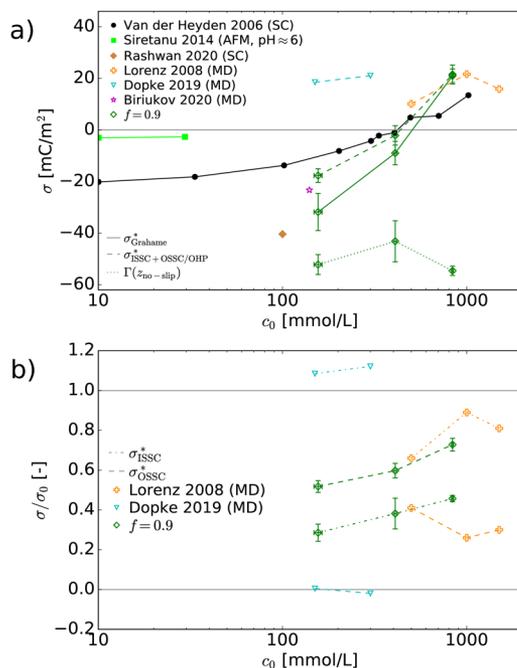
FIG. 7. (a) Differing definitions of the effective surface charge density $\sigma^*_{\text{Grahame}}$, $\Gamma(z_{\text{no-slip}})$, and $\sigma^*_{\text{ISSC+OSSC}} \approx \sigma^*_{\text{OHP}}$ from experiments and MD simulations at varying concentrations. (b) The relative charge contributions of σ^*_{ISSC} and σ^*_{OSSC} for various MD studies. The confidence intervals are 68%.

Furthermore, reasonable agreement is found across the MD studies, with the exception of our previous work.[35] However, Fig. 7(b) displays that the relative charge contribution of ISSC and OSSC differs considerably between different MD studies. We predict $\sigma_{\text{ISSC}}/\sigma_0$ between 25% and 45% and $\sigma_{\text{OSSC}}/\sigma_0$ between 50% and 75% for our concentration range, while Lorenz and Travesset,[25] for example, predict $\sigma_{\text{ISSC}}/\sigma_0$ between 65% and 90% and $\sigma_{\text{OSSC}}/\sigma_0$ between 25% and 40%. Döpke et al.[35] even predict overscreening from the ISSC contribution alone ($\sigma_{\text{ISSC}}/\sigma_0 > 1$), while the ions forming OSSC had no net contribution due to a balance between Ca^{2+} and Cl^- ions forming OSSC. These differences clearly showcase that different MD simulation force fields do not yield consistent amounts of ion adsorption without specifically tuning the force field for this property as we have essentially done in this study.

Based on our simulations corresponding to $f = 0.9$, we conclude that for realistic amorphous silica in contact with an aqueous solution of 100 mmol/l–800 mmol/l $CaCl_2$ at pH 7.5, ~25% to 45% of the ions adsorb specifically, in other words forming ISSC [see Fig. 7(b)]. The respective ion surface densities are given in Fig. S5.

C. Mobility of ions within the EDL

Until now, we have only briefly discussed dynamics when defining $z_{\text{no-slip}}$ and in relation to the slope of the ζ-potential–concentration curve. Here, we discuss the dynamics within the EDL in more detail since this is essential to parametrize a relation between measured transport and the EDL structure.

Combining our EOF simulations with kinetic theory,[75,76] we obtain the average ion transport diffusion coefficient D_k^X per ion $X \in \{Ca^{2+}, Cl^-\}$ and adsorption type $k \in \{\text{ISSC, OSSC, diff, free}\}$ following

$$D_k^X = \frac{\int \rho_{n,k}^X(z) D_k^X(z) dz}{\int \rho_{n,k}^X(z) dz}. \tag{11}$$

Here, $\rho_{n,k}^X(z)$ is the number density profile and $D_k^X(z)$ the ion transport diffusion profile given by Eq. (12) with $\mu_{q,k}^X(z)$ being the electrical mobility profile given by Eq. (13). Note that the streaming velocities $u_{x,k}^X(z)$ and $u_x^{\text{water}}(z)$ are scaled by $1/0.85$ to compensate for the scaled charges.[36] The resulting ion transport diffusion coefficients D_k^X are provided in Fig. 8,

$$D_k^X(z) = \frac{\mu_{q,k}^X(z) k_B T}{\nu e}, \tag{12}$$

$$\mu_{q,k}^X(z) = \frac{u_{x,k}^X(z) - u_x^{\text{water}}(z)}{E_x}. \tag{13}$$

In agreement with previous MD studies,[34,40,59,66] the dynamic Stern layer theory,[77–81] and the viscoelectric model,[62,63] D_k^X reduces with proximity to the surface and increasing concentration. The free ion transport diffusion coefficient D_{free}^X found here is in reasonable agreement with previously reported values for this force field of
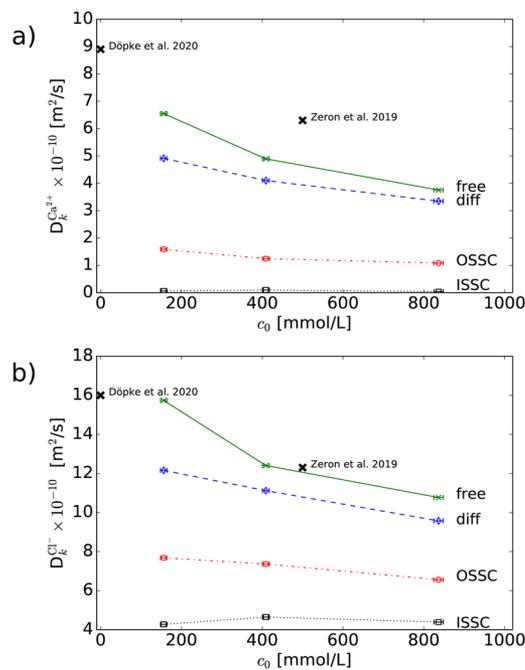
FIG. 8. Transport diffusion coefficients D_k^X based on ion adsorption types $k \in \{\text{ISSC, OSSC, diff, free}\}$ when $f = 0.9$. (a) $X = \text{Ca}^{2+}$. (b) $X = \text{Cl}^-$. The confidence intervals for the concentration are 68%. The confidence intervals for D_k^X are omitted since these exceed the axis limits.

6.3×10^{-10} and 12.3×10^{-10} m^2/s for Ca^{2+} and Cl$^-$, respectively, at 500 mmol/l and $8.9(8) \times 10^{-10}$ and $16.0(8) \times 10^{-10}$ m^2/s, respectively, at infinite dilution.[40,66] In the diffuse layer, D_{diff}^X is between 70% and 85% of D_{free}^X. For ions forming OSSC, the diffusion is further reduced to between 40% and 60% of D_{free}^X. For ions forming ISSC, we find $D_{\text{ISSC}}^{\text{Ca}^{2+}}/D_{\text{free}}^{\text{Ca}^{2+}} < 0.002$ and $D_{\text{ISSC}}^{\text{Cl}^-}/D_{\text{free}}^{\text{Cl}^-} < 0.02 - 0.06$. We attribute the difference in diffusion between Ca^{2+} and Cl$^-$ ions forming ISSC to the difference in adsorption sites. While Ca^{2+} ions adsorb specifically on negatively charged O$^-$ sites, we expect Cl$^-$ ions to adsorb specifically on either SiOH or surface Si atoms, which have their charges fully compensated by neighboring wall atoms. Consequently, the energy required to remove an adsorbed Ca^{2+} ion is greater than that required to remove an adsorbed Cl$^-$ ion.

In conclusion, for realistic amorphous silica in contact with an aqueous solution between 100 mmol/l and 800 mmol/l CaCl$_2$ at pH 7.5, the diffuse layer clearly possesses a reduced mobility, questioning the use of bulk transport properties throughout the diffuse layer as is done in most continuum models (Gouy–Chapman and basic Stern models, for example). Furthermore, Ca^{2+} ions forming ISSC can be considered as virtually immobile. However, the same assumption is not valid for Cl$^-$ ions forming ISSC nor for Ca^{2+} and Cl$^-$ ion forming OSSC. However, the usual assumption of an immobile Stern layer (containing ISSC and OSSC) may yield seemingly correct results if the reduced mobility in the diffuse layer is compensated by a finite mobility of ions within the Stern layer.

IV. CONCLUSION

We have shown that the experimentally measured concentration at which the ζ-potential equals zero in a silica slit pore filled with a CaCl$_2$ electrolyte at pH 7.5 can be reproduced in EOF MD simulations. This concentration that we called isoelectric concentration (IEC) was argued to be least susceptible to modeling errors, thus providing a suitable experimental reference point to benchmark non-equilibrium MD simulations. We demonstrated that it cannot be taken for granted that MD force fields automatically reproduce correct and consistent EDL properties. For example, previous MD studies have shown inconsistent amounts of ion adsorption, with most of them predicting an abundance of ISSC formation and thus underpredicting the experimental IEC.[25,26,35] We believe that, to a great extent, this is caused by the fact that ion–surface interactions are typically not optimized or validated, but rather computed from standard mixing rules. Our data show that ion adsorption is extremely sensitive to the ion–surface interaction, and we presented an approach in which this interaction was tuned to obtain the right amount of specifically adsorbed ions necessary to reproduce the IEC.

The slope of the ζ-potential against concentration between 100 mmol/l and 800 mmol/l varies between different experiments and simulations. Based on the rather consistent isoelectric point and concentration, we argue that the differences in slope are not caused by differences in surface sample conditions, but rather by modeling errors. We discussed various possible modeling errors that could bias the information obtained from experiments or simulations. One reason could be that the fluid transport properties in simulations and experiments differ. For example, different channel widths can lead to differences in the viscosity. Also, the force field used is known to slightly underpredict the experimental viscosity of water. Another concern may be the fact that electrostatic screening is not considered by non-polarizable force fields. The scaled charges of the Madrid-2019 ions account for the electrostatic screening in bulk water simulations, but the effect and validity of scaled charges in confinement still needs to be evaluated in more detail.[41]

The diffusion coefficients of ions forming ISSC, OSSC, those within the diffuse layer, and free ions were calculated to assess the validity of the common assumption of an immobile Stern layer and the use of bulk transport values in the diffuse layer. It was found that for Cl$^-$ ions no clear immobile layer can be found, while for Ca^{2+} ions the ISSC layer is virtually immobile. This difference is attributed to the adsorption sites of Ca^{2+} and Cl$^-$. Despite ions forming OSSC frequently being classified as immobile, we found these do have a diffusion coefficient ranging from 40% to 60% of D_{free}^X. Finally, the ions within the diffuse layer, which are commonly classified as fully mobile, were found to present a reduced diffusion as low as 70% of D_{free}^X. These findings clearly oppose the traditional interpretation of the immobile Stern layer and the bulk like diffuse layer. However, the deficit in the diffuse layer may be compensated by the finite diffusion in the Stern layer.

The findings in this study have wide reaching implications in improving the understanding and interpretation of experiments in which the results depend on the EDL structure and dynamics. For example, empirical surface complexation models provide estimates of properties within the Stern layer and thereby boundary conditions for a continuum model spanning the diffuse and bulk regions. Most of these models require the specification of the Stern layer capacitance. With the right distribution of ions within the Stern layer given by detailed MD simulations, this capacitance can now be calculated accurately.

Finally, our results can be used to supplement experimental findings where direct measurement or unambiguous interpretation is not possible. Albeit the simulations presented here are at relatively high concentrations, the scaling parameter derived here is thought to be also valid at lower concentrations. One way of verifying this could be to use the isoelectric point when comparing experiments and simulations. This is the pH at which $\zeta = 0$ when the concentration is kept constant, which consequently results in a similar reduction of errors as for the IEC. In fact, one can find the isoelectric point and concentration for any pH or any concentration by varying the concentration or pH, respectively, providing an infinite number of unambiguous points.

SUPPLEMENTARY MATERIAL

Additional equations and figures are provided in the supplementary material.

ACKNOWLEDGMENTS

DATA AVAILABILITY

The data that support the findings of this study are available from the corresponding author upon reasonable request.

REFERENCES

[1] M. H. Badizad, M. M. Koleini, R. Hartkamp, S. Ayatollahi, and M. H. Ghazanfari, J. Colloid Interface Sci. **575**, 337 (2020).

[2] B. Jeon, S. K. R. S. Sankaranarayanan, A. C. T. van Duin, and S. Ramanathan, J. Chem. Phys. **134**, 234706 (2011).

[3] B. M. Lowe, Y. Maekawa, Y. Shibuta, T. Sakata, C.-K. Skylaris, and N. G. Green, Phys. Chem. Chem. Phys. **19**, 2687 (2017).

[4] D. Bohra, J. H. Chaudhry, T. Burdyny, E. A. Pidko, and W. A. Smith, Energy Environ. Sci. **12**, 3380 (2019).

[5] J. Lyklema, Fundamentals of Interface and Colloid Science: Soft Colloids (Elsevier, 2005), Vol. 5.

[6] R. Sivakumarasamy, R. Hartkamp, B. Siboulet, J.-F. Dufrêche, K. Nishiguchi, A. Fujiwara, and N. Clément, Nat. Mater. **17**, 464 (2018).

[7] J. Lützenkirchen, T. Preočanin, D. Kovačević, V. Tomišić, L. Lövgren, and N. Kallay, Croat. Chem. Acta **85**, 391 (2012).

[8] I. Siretanu, D. Ebeling, M. P. Andersson, S. S. Stipp, A. Philipse, M. C. Stuart, D. van den Ende, and F. Mugele, Sci. Rep. **4**, 4956 (2014).

[9] F. H. J. van der Heyden, D. Stein, K. Besteman, S. G. Lemay, and C. Dekker, Phys. Rev. Lett. **96**, 224502 (2006).

[10] T. Lagström, T. A. Gmür, L. Quaroni, A. Goel, and M. A. Brown, Langmuir **31**, 3621 (2015).

[11] Z. Zhang, P. Fenter, L. Cheng, N. C. Sturchio, M. J. Bedzyk, M. Předota, A. Bandura, J. D. Kubicki, S. N. Lvov, P. T. Cummings, A. A. Chialvo, M. K. Ridley, P. Bénézeth, L. Anovitz, D. A. Palmer, M. L. Machesky, and D. J. Wesolowski, Langmuir **20**, 4954 (2004).

[12] M. S. Azam, A. Darlington, and J. M. Gibbs-Davis, J. Phys.: Condens. Matter **26**, 244107 (2014).

[13] J. Lützenkirchen, T. Scharnweber, T. Ho, A. Striolo, M. Sulpizi, and A. Abdelmonem, J. Colloid Interface Sci. **529**, 294 (2018).

[14] O. Theodoly, L. Cascão-Pereira, V. Bergeron, and C. J. Radke, Langmuir **21**, 10127 (2005).

[15] P. Leroy, N. Devau, A. Revil, and M. Bizi, J. Colloid Interface Sci. **410**, 81 (2013).

[16] T. A. Gmür, A. Goel, and M. A. Brown, J. Phys. Chem. C **120**, 16617 (2016).

[17] A. V. Delgado, F. González-Caballero, R. J. Hunter, L. K. Koopal, and J. Lyklema, J. Colloid Interface Sci. **309**, 194 (2007), part of special issue on: elkin 06, International Electrokinetics Conference, June 25–29, Nancy, France.

[18] S. Li, P. Leroy, F. Heberling, N. Devau, D. Jougnot, and C. Chiaberge, J. Colloid Interface Sci. **468**, 262 (2016).

[19] A. Szymczyk, P. Fievet, M. Mullet, J. C. Reggiani, and J. Pagetti, J. Membr. Sci. **143**, 189 (1998).

[20] G. Hurwitz, G. R. Guillen, and E. M. V. Hoek, J. Membr. Sci. **349**, 349 (2010).

[21] Z. Brkljača, D. Namjesnik, J. Lützenkirchen, M. Předota, and T. Preočanin, J. Phys. Chem. C **122**, 24025 (2018).

[22] A. M. Darlington, T. A. Jarisz, E. L. DeWalt-Kerian, S. Roy, S. Kim, M. S. Azam, D. K. Hore, and J. M. Gibbs, J. Phys. Chem. C **121**, 20229 (2017).

[23] M. M. Sartin, W. Sung, S. Nihonyanagi, and T. Tahara, J. Chem. Phys. **149**, 024703 (2018).

[24] R. Hartkamp, A.-L. Biance, L. Fu, J.-F. Dufrêche, O. Bonhomme, and L. Joly, Curr. Opin. Colloid Interface Sci. **37**, 101 (2018).

[25] C. D. Lorenz and A. Travesset, Phys. Rev. E **75**, 061202 (2007).

[26] C. D. Lorenz, P. S. Crozier, J. A. Anderson, and A. Travesset, J. Phys. Chem. C **112**, 10222 (2008).

[27] H. Zhang, A. A. Hassanali, Y. K. Shin, C. Knight, and S. J. Singer, J. Chem. Phys. **134**, 024705 (2011).

[28] N. R. Haria and C. D. Lorenz, Phys. Chem. Chem. Phys. **14**, 5935 (2012).

[29] S. Dewan, V. Carnevale, A. Bankura, A. Eftekhari-Bafrooei, G. Fiorin, M. L. Klein, and E. Borguet, Langmuir **30**, 8056 (2014).

[30] N. R. Haria and C. D. Lorenz, J. Phys. Chem. C **119**, 12298 (2015).

[31] R. Hartkamp, B. Siboulet, J.-F. Dufrêche, and B. Coasne, Phys. Chem. Chem. Phys. **17**, 24683 (2015).

[32] S. Hocine, R. Hartkamp, B. Siboulet, M. Duvail, B. Coasne, P. Turq, and J.-F. Dufrêche, J. Phys. Chem. C **120**, 963 (2016).

[33] S. Prakash, H. A. Zambrano, K. K. Rangharajan, E. Rosenthal-Kim, N. Vasquez, and A. T. Conlisk, Microfluid. Nanofluid. **20**, 8 (2016).

[34] B. Siboulet, S. Hocine, R. Hartkamp, and J.-F. Dufrêche, J. Phys. Chem. C **121**, 6756 (2017).

[35] M. F. Döpke, J. Lützenkirchen, O. A. Moultos, B. Siboulet, J.-F. Dufrêche, J. T. Padding, and R. Hartkamp, J. Phys. Chem. C **123**, 16711 (2019).

[36] D. Biriukov, P. Fibich, and M. Předota, J. Phys. Chem. C **124**, 3159 (2020).

[37] R. M. Venable, Y. Luo, K. Gawrisch, B. Roux, and R. W. Pastor, J. Phys. Chem. B **117**, 10183 (2013).

[38] D. Biriukov, O. Kroutil, and M. Předota, Phys. Chem. Chem. Phys. **20**, 23954 (2018).

[39] I. Leontyev and A. Stuchebrukhov, Phys. Chem. Chem. Phys. **13**, 2613 (2011).

[40] I. M. Zeron, J. L. F. Abascal, and C. Vega, J. Chem. Phys. **151**, 134504 (2019).

[41] E. Duboué-Dijon, M. Javanainen, P. Delcroix, P. Jungwirth, and H. Martinez-Seara, J. Chem. Phys. **153**, 050901 (2020).

[42] K. Szymanek, R. Charmas, and W. Piasecki, Chemosphere **242**, 125162 (2020).

[43] A. Yaroshchuk and V. Ribitsch, Langmuir **18**, 2036 (2002).

[44] D. Lis, E. H. G. Backus, J. Hunger, S. H. Parekh, and M. Bonn, Science **344**, 1138 (2014).

[45] B. L. Werkhoven, J. C. Everts, S. Samin, and R. van Roij, Phys. Rev. Lett. **120**, 264502 (2018).

[46] B. W. H. van Beest, G. J. Kramer, and R. A. van Santen, Phys. Rev. Lett. **64**, 1955 (1990).

[47] F. S. Emami, V. Puddu, R. J. Berry, V. Varshney, S. V. Patwardhan, C. C. Perry, and H. Heinz, Chem. Mater. **26**, 2647 (2014).

[48] J. L. F. Abascal and C. Vega, J. Chem. Phys. **123**, 234505 (2005).

[49] A. Riese, "Adsorption of radium and thorium onto quartz and kaolinite: A comparison of solution/surface equilibria models," Ph.D. thesis, Colorado School of Mines, Boulder, CO, 1982.

[50] M. Karlsson, C. Craven, P. M. Dove, and W. H. Casey, Aquat. Geochem. **7**, 13 (2001).

[51] A. T. Celebi and A. Beskok, J. Phys. Chem. C **122**, 9699 (2018).

[52] A. T. Celebi, B. Cetin, and A. Beskok, J. Phys. Chem. C **123**, 14024 (2019).

[53] S. Plimpton, J. Comput. Phys. **117**, 1 (1995).

[54] R. W. Hockney and J. W. Eastwood, *Computer Simulation Using Particles* (Hilger, 1989).

[55] J.-P. Ryckaert, G. Ciccotti, and H. J. C. Berendsen, J. Comput. Phys. **23**, 327 (1977).

[56] I.-C. Yeh and M. L. Berkowitz, J. Chem. Phys. **111**, 3155 (1999).

[57] H. A. Lorentz, Ann. Phys. **248**, 127 (1881).

[58] S. ben Jabrallah, F. Malloggi, L. Belloni, L. Girard, D. Novikov, C. Mocuta, D. Thiaudière, and J. Daillant, Phys. Chem. Chem. Phys. **19**, 167 (2017).

[59] I. C. Bourg and G. Sposito, J. Colloid Interface Sci. **360**, 701 (2011).

[60] M. Rashwan, B. Rehl, A. Sthoer, A. Darlington, M. S. Azam, H. Zeng, Q. Liu, E. Tyrode, and J. Gibbs, J. Phys. Chem. C **124**, 26973 (2020).

[61] A. Zaragoza, M. A. Gonzalez, L. Joly, I. López-Montero, M. A. Canales, A. L. Benavides, and C. Valeriani, Phys. Chem. Chem. Phys. **21**, 13653 (2019).

[62] W.-L. Hsu, H. Daiguji, D. E. Dunstan, M. R. Davidson, and D. J. E. Harvie, Adv. Colloid Interface Sci. **234**, 108 (2016).

[63] W.-L. Hsu, D. J. E. Harvie, M. R. Davidson, D. E. Dunstan, J. Hwang, and H. Daiguji, J. Phys. Chem. C **121**, 20517 (2017).

[64] M. Rezaei, A. R. Azimian, A. R. Pishevar, and D. J. Bonthuis, Phys. Chem. Chem. Phys. **20**, 22517 (2018).

[65] F. Liu, A. Klaassen, C. Zhao, F. Mugele, and D. van den Ende, J. Phys. Chem. B **122**, 933 (2018).

[66] M. F. Döpke, O. A. Moultos, and R. Hartkamp, J. Chem. Phys. **152**, 024501 (2020).

[67] M. Laliberté and W. E. Cooper, J. Chem. Eng. Data **49**, 1141 (2004).

[68] M. Laliberté, J. Chem. Eng. Data **54**, 1725 (2009).

[69] Y. Marcus, *Ion Properties* (CRC Press, 1997).

[70] D. C. Grahame, Chem. Rev. **41**, 441 (1947).

[71] H. Butt, K. Graf, and M. Kappl, *Physics and Chemistry of Interfaces* (John Wiley & Sons, 2006).

[72] L. Boltzmann, Wiss. Abh. **1**, 49 (1868).

[73] J. Lutzenkirchen, *Surface Complexation Modelling* (Elsevier, 2006).

[74] R. J. Hunter, *Zeta Potential in Colloid Science: Principles and Applications* (Academic Press, 2013), Vol. 2.

[75] W. Sutherland, London, Edinburgh Dublin Philos. Mag. J. Sci. **9**, 781 (1905).

[76] A. Einstein, Ann. Phys. **322**, 549 (1905).

[77] C. F. Zukoski and D. A. Saville, J. Colloid Interface Sci. **107**, 322 (1985).

[78] J. Lyklema, Colloids Surf., A **92**, 41 (1994), Part of special issue on: A Collection of Papers Presented at the International Symposium on Elektrokinetic Phenomena '93.

[79] S. S. Dukhin, Adv. Colloid Interface Sci. **61**, 17 (1995).

[80] S. S. Dukhin, R. Zimmermann, and C. Werner, Colloids Surf., A **195**, 103 (2001).

[81] F. J. Rubio-Hernández, F. Carrique, and E. Ruiz-Reina, Adv. Colloid Interface Sci. **107**, 51 (2004).